Inelastic x-ray scattering in heterostructures: electronic excitations in $LaAlO_3/SrTiO_3$

2015 J. Phys.: Condens. Matter 27 335501

(http://iopscience.iop.org/0953-8984/27/33/335501)

IOP Publishing Journal of Physics: Condensed Matter

J. Phys.: Condens. Matter **27** (2015) 335501 (10pp) doi:10.1088/0953-8984/27/33/335501

Inelastic x-ray scattering in heterostructures: electronic excitations in $LaAlO_3/SrTiO_3$

Kari O Ruotsalainen[1], Christoph J Sahle[1,2], Tobias Ritschel[3], Jochen Geck[3], Masayuki Hosoda[4,5], Christopher Bell[4,9], Yasuyuki Hikita[4], Harold Y Hwang[4,6], Tim T Fister[7], Robert A Gordon[8,10], Keijo Hämäläinen[1], Mikko Hakala[1] and Simo Huotari[1]

[1] Department of Physics, University of Helsinki, PO Box 64, FI-00014, Finland
[2] European Synchrotron Radiation Facility, B.P. 220, F-38043 Grenoble cedex 9, France
[3] Leibniz Institute for Solid State and Material Research IFW Dresden, Helmholtzstrasse 20, D-01069 Dresden, Germany
[4] Stanford Institute for Materials and Energy Sciences, SLAC National Accelerator Laboratory, Menlo Park, CA 94025, USA
[5] Department of Advanced Materials Science, University of Tokyo, Kashiwa, Chiba 277-8561, Japan
[6] Geballe Laboratory for Advanced Materials, Department of Applied Physics, Stanford University, Stanford, CA 94305, USA
[7] Chemical Sciences and Engineering Division, Argonne National Laboratory, Argonne, IL 60439, USA
[8] PNCSRF/CLS, APS Sector 20, Argonne, IL, USA

E-mail: kari.ruotsalainen@helsinki.fi

Received 27 March 2015, revised 17 June 2015
Accepted for publication 23 June 2015
Published 29 July 2015

Abstract

We present an investigation of the valence-electron excitation spectra including the collective plasmon modes of $SrTiO_3$, $LaAlO_3$ and their heterostructures with non-resonant inelastic x-ray scattering. We analyse the spectra using calculations based on first principles and atomic multiplet models. We demonstrate the feasibility of performing valence IXS experiments in a total reflection geometry. Surprisingly, we find that the plasmon, interband and semicore excitations in multilayers are well described as a superposition of bulk-compound spectra even in a superstructure composing of layers of only one atomic layer thickness.

Keywords: inelastic x-ray scattering, heterostructures, electronic structure

(Some figures may appear in colour only in the online journal)

Introduction

Non-resonant inelastic x-ray scattering (IXS) is a versatile probe of charge neutral excitations in condensed matter. Typical applications include investigations of valence electron excitations and shallow core absorption edges in bulk solids [1–12]. The scattering process can excite collective modes such as phonons and plasmons, and various types of particle–hole excitations. A notable merit of IXS lies in the high energies of the incident and scattered radiation. Penetration into and out of complex sample environments can be achieved. Moreover, the momentum transfer in the scattering process is essentially controlled by the incident energy and scattering angle. The dispersion of excitations can thus be studied, and non-dipolar transitions are readily excited at large momentum transfers. Considering the recent interest in transition metal oxide films and heterostructures, IXS offers new possibilities in the study of electronic structure and excitations of these systems.

Hard x-ray IXS experiments have been focused on bulk systems. The high incident photon energies (typically 5–10 keV)

[9] Current address: H H Wills Physics Laboratory, University of Bristol, Bristol, BS8 1TL, UK
[10] Department of Physics, Simon Fraser University, Burnaby, BC V5A 1S6, Canada

naturally explain this. For example 10 keV photons penetrate several microns even into the densest known compounds and elements. Thus the use of a grazing incidence or total reflection scattering geometry is necessary when studying film like samples with IXS. The feasibility of investigating thin films with IXS has been recently demonstrated by the observations of core excitations in a 10 nm $La_{0.6}Sr_{0.4}CoO_3$ film by Fister *et al* and phonon spectra in 2H-$NbSe_2$ [13, 14]. Following these groundbreaking investigations, we present experimental results and computational analysis on the valence IXS spectra in $LaAlO_3/SrTiO_3$ (LAO/STO) heterostructures and bulk crystals of LAO and STO.

The IXS cross section is theoretically quite well understood and calculable from first principles (see, e.g. [15]). The doubly differential cross section is written as

$$\frac{\mathrm{d}^2\sigma}{\mathrm{d}\Omega \mathrm{d}\omega} = r_0^2(\vec{e}_1 \cdot \vec{e}_2)\frac{\omega_2}{\omega_1}S(\vec{q},\omega), \quad (1)$$

where r_0 is the classical electron radius, while $\vec{e}_{1(2)}$ and $\omega_{1(2)}$ are the polarization vectors and energies of the incident (scattered) radiation, respectively. $S(\vec{q},\omega) = \sum_{i,f} |\langle f|\mathrm{e}^{\mathrm{i}\vec{q}\cdot\vec{r}_i}|g\rangle|^2 \delta(E_g - E_i - \hbar\omega)$ is the dynamic structure factor, where the summation runs over all electrons, denoted by i, in the system and all final states $|f\rangle$, and $\langle g|$ is the ground state. $S(\vec{q},\omega)$ is related to the imaginary part of the macroscopic inverse dielectric function

$$S(\vec{q},\omega) = \frac{q^2}{4\pi^2 e^2 n}\,\mathrm{Im}\left[\frac{-1}{\varepsilon(\vec{q},\omega)}\right], \quad (2)$$

where n is the average electron density and e is the unit charge.

LAO and STO are insulating perovskite oxides with band gaps of 3.2 and 5.6 eV, respectively. The ground state electronic structures of both compounds are moderately well described with density functional theory (DFT) in the local density approximation (LDA) [16, 17]. Although the band gaps are underestimated, a spin unpolarized LDA treatment produces an insulating ground state. For STO, a recent G_0W_0 calculation resulted in a Γ point band gap of 3.76 eV in good agreement with experiment [18]. Ohtomo and Hwang showed that surprisingly, if 4–5 unit cells of LAO are grown on a TiO_2 terminated STO(1 0 0) substrate, the interface becomes conducting [19, 20]. The formed electron gas has a large mobility and may have applications in oxide electronics [21, 22]. Furthermore, the interface may provide a tunable platform for studying the fundamental physics of (quasi) two dimensional electron systems. Subsequent investigations revealed that the interface can also exhibit superconductivity, ferromagnetism and their phase separated coexistence at cryogenic temperatures [23–27]. The initial discovery raised a surge of investigations on the atomic and electronic structure effects affecting the metallization of the interface [28–30]. A polar catastrophe scenario was presented to explain the interface conductivity. In this scenario electrons are promoted to conduction states to the Ti 3*d* bands at the interface to screen a divergence in the Hartree potential induced by the polar LAO layers in analogy with semiconductor multilayers [19, 31]. The effects of intrinsic and extrinsic oxygen vacancies and cation mixing across the interface have also been considered [28, 32, 33]. Overall the interface presents a complicated problem in which the roles of stoichiometry, atomic geometries and electronic structure need to be understood. In this work we focus on the electronic excitation spectra of LAO/STO heterostructures via an comparison with bulk spectra.

The properties of STO in bulk and film forms are fascinating in their own right. STO crystallizes to a cubic perovskite structure with the space group $Pm\bar{3}m$. It exhibits a rich phase diagram in temperature, doping and pressure or strain. STO undergoes a cubic to tetragonal phase transition at 105 K and exhibits quantum paraelectricity at 0.35–4 K [34]. Superconductivity can be introduced via creation of oxygen vacancies or Nb doping [35, 36]. In thin films, interfacial room temperature ferroelectricity in strained STO has also been observed [37]. Here we choose to study superlattice samples, as their thickness is well suited for hard x-rays.

The inverse dielectric function of LAO/STO multilayers has been studied with electron energy loss spectroscopy (EELS) in the core excitation regime, providing important information on the interface geometry and stoichiometry [38]. However the valence excitation regime has not been studied so far with either IXS or EELS. Our experiment provides new information on the evolution the electronic structure of LAO and STO as they form a heterostructure. The experimental and computational valence and core electron excitation spectra in LAO/STO systems will be presented in the following.

Experimental methods and samples

Three LAO/STO heterostructures with varying superlattice stacking were investigated using IXS. All samples were grown by pulsed laser deposition on TiO_2 terminated STO(1 0 0) substrates. Oxygen partial pressure of 10^{-5} Torr was used. Layer-by-layer growth was verified with *in situ* electron scattering, and *ex situ* x-ray diffraction demonstrated the presence of superlattice peaks. See [39] for further details. The superlattice stackings were 1 ML LAO/1 ML STO, 2 ML LAO/2 ML STO and 5 ML LAO/5 ML STO, where ML denotes a single unit cell thickness. The total thicknesses of the structures, approximated from bulk lattice constants, were 55 nm. The samples will be denoted ML1, ML2 and ML5, respectively. The bulk crystals were obtained from MaTeck GmbH.

The IXS experiments were performed at beamline 20-ID of the Advanced Photon Source. The undulator spectrum was monochromatized with a Si(1 1 1) double crystal setup. The radiation from the monochromator was then focused onto the sample using a Kirkpatrick–Baez mirror. The spectra of scattered x-rays were collected using the LERIX spectrometer [40]. We used 19 spherically bent Si(1 1 1) crystal analysers. The energy loss measurements were performed with the inverse energy scan technique, where the incident energy is scanned while keeping the scattered photon energy fixed at

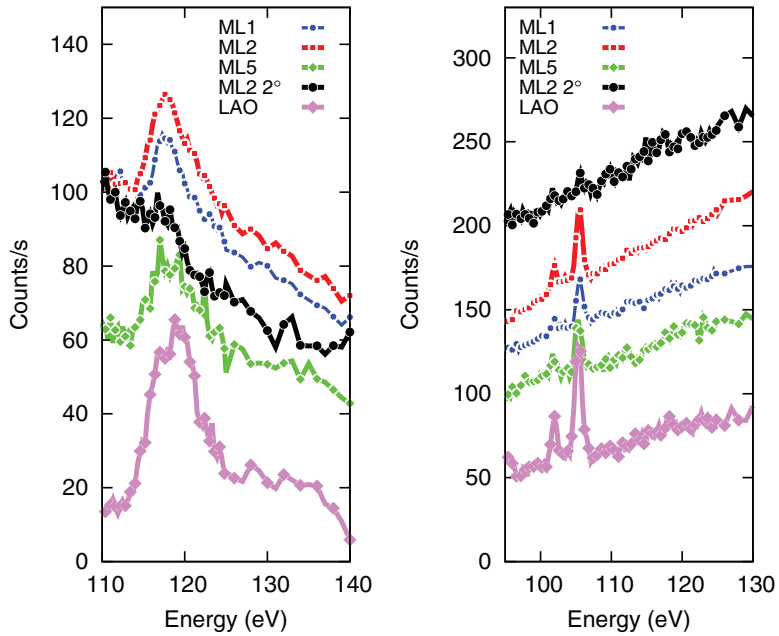

Figure 1. La $N_{4,5}$ structures from different data sets in GI-TR and non-GI conditions. Left panel: average over values of Q ranging between 1–3 Å^{-1} showing approximately the dipole limit spectra. Right panel: average over values of Q 4–8 Å^{-1} representing higher order multipole spectra. The 2-uc spectra are also shown in non-GI geometry (incidence angle of 2°), which represents the bulk STO substrate spectrum without significant multilayer contribution.

7.912 keV. The combined band passes of the monochromator and spectrometer sum up to a total energy resolution of 1 eV. The total reflection conditions were verified with a post-sample phosphor screen by visually observing the appearance of total reflection scattering intensity at grazing angles below 0.5°. During the total reflection scans, the samples were inclined at an angle of 0.2°–0.3° with respect to the incident beam.

The spectra were measured repeatedly, normalized to the incident beam intensity, and checked for internal consistency. The consistent scans were finally averaged. The valence spectra were processed by subtracting a Pearson VII distribution from the experimental data to mimic the tail of the elastic line. Our data are then considered reliable above 5 eV. For comparison purposes, the spectra then were normalized to unit area over the fixed energy interval of 25–50 eV.

To prove that the IXS measurements indeed probe the multilayer structure, figure 1 shows the La $N_{4,5}$ core-excitations spectra from LAO/STO multilayer, and from bulk $LaAlO_3$. We measured the spectra both in grazing-incidence total reflection (GI-TR) and in non-GI (incidence angle 2°) geometries. This energy region has no spectral features from STO, so the observed peaks can only originate from LAO. The spectra from other La compounds are known to exhibit a giant dipole resonance at ∼120 eV at low momentum transfers, and sharp non-dipolar multiplet peaks at lower energies (100–110 eV) that dominate the spectra at large momentum transfer ($q > 4$ Å^{-1}) [12]. All spectra correspond to the La $4d \rightarrow 4f$ transitions. It can be seen in figure 1 that the La spectra, which can only originate from the multilayer, are clearly visible in the GI-TR conditions, while it nearly disappears at non-GI. Comparing to bulk LAO it can be estimated that 50% of the signal originates from the multilayer, the rest coming deeper from the substrate. As we will show later in this article, the same conclusion will be reached via principal component fitting of multilayer spectra with bulk reference spectra.

Computational methods

First principles calculations

The ground state electronic structures of LAO and STO were calculated using the DFT plane wave pseudopotential method as implemented in the ABINIT package [41]. The LDA was used to account for exchange and correlation effects. Norm-conserving Hartwigensen–Goedecker–Hutter pseudopotentials with semicore states were used [42]. The atomic states included in the valence were Sr-4*s*/4*p*/5*s*, Ti-3*s*/3*p*/3*d*/4*s* La-5*s*/5*p*/5*d*/6*s*, Al-3*s*/3*p* and O-2*s*/2*p*. The experimental cubic lattice constant $a_{STO} = 3.905$ Å was used for STO [43]. A pseudocubic structure with $a_{LAO} = 3.7191$ Å was used for LAO [44]. The total energies were found to be converged at a kinetic energy cutoff of 80 Ha. We used an unshifted $8 \times 8 \times 8$ Monkhorst–Pack grid with 56 k-points in the irreducible Brillouin zone. The resulting indirect and direct gaps were 1.9 and 2.3 eV STO, and 3.5 and 3.6 eV for LAO, in agreement with previous LDA calculations [17, 45, 46]. The site- and symmetry-resolved density of states (DOS) were also calculated to aid in the interpretation of the excitation spectra. The tetrahedron method was used in the Brillouin zone integrations. The integration radii in STO were set as $r_{Sr} = 2.607$ atomic units (a.u.), $r_{Ti} = 1.530$ a.u., and $r_O = 2.840$ a.u, as in [18]. For LAO, an integration radius of 2 a.u. was used for all atoms.

The macroscopic dielectric functions in the energy range of 0–50 eV were evaluated in the random phase approximation (RPA) using the yambo code [15, 47]. The number of bands included in the polarization function was 120. The local field effects were taken into account by inverting the dielectric matrix with 300 $\vec{G}$ components. The spectra were found to be converged with respect to the number of bands and local field effects. We used a constant quasiparticle lifetime of 0.5 eV in evaluating the response function.

The dielectric function was evaluated at $\vec{q} = (0.5\vec{a}^*, 0, 0.08\vec{c}^*)$. The purpose of the computation is not to analyze the full $(\vec{q}, \omega)$ dependence of the response functions, but to aid in identification of excitations. This procedure naturally means that the energies of dispersive features, such as plasmons, are not directly comparable. On the other hand, non-dispersive excitations involving semicore states or flat bands allow for a comparison to be made.

Free-ion multiplet calculations

A set of calculations for shallow-core spectra were done using Cowan's code [48]. We assumed free ions neglecting crystal field effects, and performed the calculations in the intermediate spin–orbit coupling. The former assumption is discussed further in the next section. The calculations used the Hartree–Fock approximation with relativistic corrections. We used a 80% scaling of the Slater–Condon parameters, while the *ab initio* value was used for the spin–orbit interaction.

Intense high-order multipole excitations in core-level pre-edges measured by IXS have been found by Sternemann *et al* and thoroughly investigated and explained by Gordon *et al* [5, 12, 49]. Since then such multiplet IXS spectra have been investigated in detail in transition metals, actinides, and rare earths [5–11, 50–53].

The theory for shallow-core to valence excitations in cases where the orbitals involved in the transition share the same principal quantum number was developed by Sen Gupta *et al* [8]. According to this theory, large differences are expected between the dipole and higher-order multipole transitions. In particular, as often turns out to be the case, the multipole transitions that are lower in energy than the dipolar ones, correspond to well bound states and can be modeled using local single-ion or cluster-like models. In contrast, often dipole allowed virtual-bound resonances (such as the giant dipole resonance in rare earths) hybridize with the continuum states and are broadened into a Fano lineshape [5]. For this reason the dipole and high-order multipole excitations are treated differently in our discussion below.

Using the multiplet calculations, we consider the following excitations: Sr $4p^6 4d^0 \rightarrow 4p^5 4d^1$ ($N_{2,3}$), $4s^2 4d^0 \rightarrow 4s^1 4d^1$ (N_1), Ti $3p^6 3d^0 \rightarrow 3p^5 3d^1$ ($M_{2,3}$), and Ti $3s^2 3d^0 \rightarrow 3s^1 3d^1$ (M_1). The $p \rightarrow d$ excitations are possible via momentum channels $k = 1$ and $k = 3$ (dipole and octupole) while $s \rightarrow d$ excitations are possible via $k = 2$ (quadrupole). The valence-electron response is represented at low momentum transfers by a plasmon excitation that gradually transforms into a Compton profile with an increasing momentum transfer [3]. This, in practice, yields a relatively broad but momentum-dependent continuum-like contribution that lies below the well-defined shallow-core excitations. In order to take it into account for better comparison between the multiplet calculations and the experimental spectra, this contribution was simulated by using a free-electron gas response within the random phase approximation as detailed by Schülke [54, 55].

Results and discussion

In this section we will discuss the experimental results in comparison with the multiplet and first principles calculations. The effect of crystal fields on the shallow core excitations we observe in the $S(\vec{q}, \omega)$ is commented in the following paragraph. The experimental spectra and multiplet calculations are presented in figures 2 and 3. The valence band density of states and selected valence excitation spectra are presented alongside the calculated RPA dielectric and loss functions in figures 4–7.

Our calculations in the multiplet model neglect crystal field effects (crystal field splitting between Ti e_g and t_{2g} states is approximately 2 eV [18]) on the semicore excitations. We note that x-ray absorption studies on LAO/STO samples have revealed clear crystal field splittings that evolve with superlattice stacking (or film thickness) at the Ti $L_{2,3}$ edge [56]. Similar effects are in principle observable at the M edges of Ti as well. Gordon *et al* [57] have shown that the octupole transitions at transition metal $M_{2,3}$-edges display q-dependent energy shifts that can be traced to anisotropy of the electronic structure even in powder samples, i.e. one could expect to see a peak position shift signifying changes in the crystal field. However, one should also note that the lifetime broadenings of the Ti M_2 and M_3 states are approximately 1.2 eV [58]. Moreover, La has semicore excitations that overlap with the excitations in STO. The lifetime broadenings and line overlaps in the spectra make crystal field splittings of minor importance. Especially in the case of the La $4f$ states their effect is expected to be small. Thus we can neglect crystal field effects in the present spectral analysis.

Figure 2(a) shows the measured spectra for STO. Similar data have been obtained by valence-electron EELS by van Benthem *et al* [16]. They interpreted the spectral features in detail using band structure and density of states calculations. First, we use the ionic model with multiplet calculations to interpret some of the transitions: this aids in fingerprinting the origins of each peak. Hence in figure 2(b) we show our results from the free-ion multiplet calculations.

At lowest q, the spectra are characterised by three peaks (16 eV, 30 eV, and 50 eV). The peak at 16 eV is an interband excitation from predominantly O $2s$ to the unoccupied states. At increased values of q, the spectra gain broad weight culminating at a large peak at 50 eV at $q = 1.9 \times 2\pi/a_{\mathrm{sto}}$ This structure is attributed to a plasmon mode (although overdamped) that transforms gradually into a Compton line at high q [3, 59, 60]. The electrons that contribute to the bulk plasmon, and are considered to be in the valence, are Sr $4p$ and $5s$, Ti $3p$ and $3d$, and finally O $2s$ and $2p$. This yields a value of the electron gas

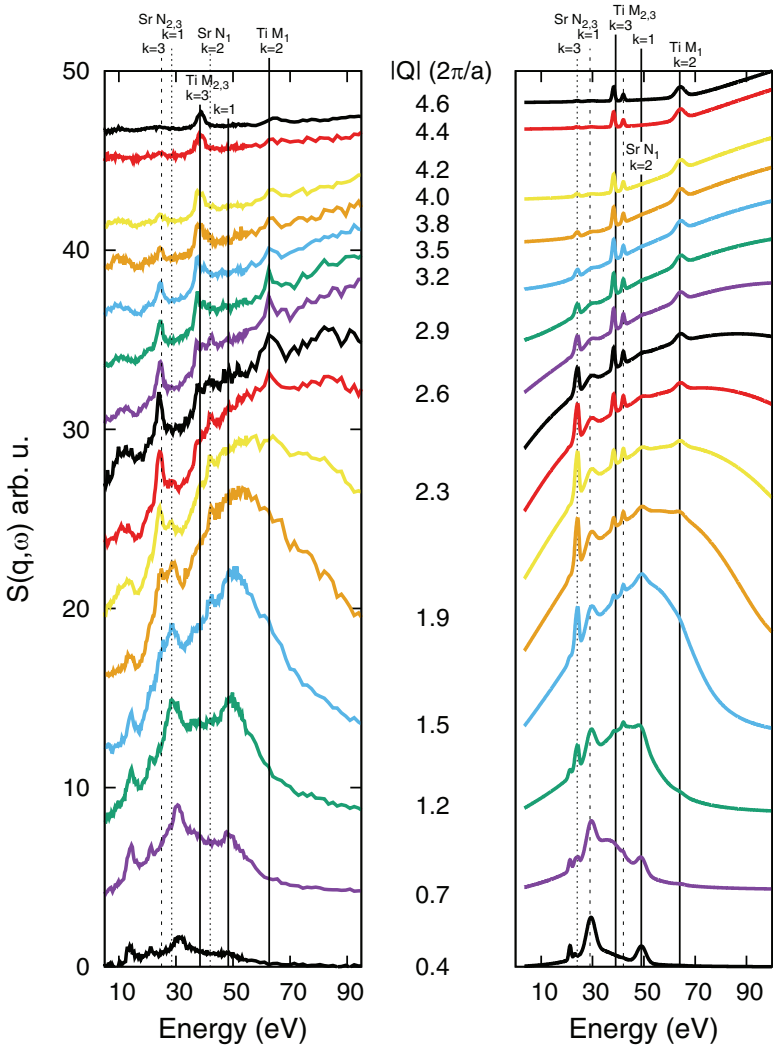

Figure 2. (a) Experimental IXS spectra of $SrTiO_3$. (b) Simulated spectrum including a plasmon/Compton lineshape, and transitions from ionic model as described in the text. Spectra are vertically offset by numbers proportional to $|\vec{q}|^2$. Note that the spectrometer chamber is filled with He and the peak at 21 eV originates from the He 1*s*–2*p* transition. The solid and dashed lines mark notable Ti and Sr semicore excitations, respectively.

density parameter $r_s = 1.39$ and the plasmon energy at $q = 0$ of 28.9 eV. However, the plasmon is strongly damped and has a width of ∼10 eV. Furthermore, the peak seen at 30 eV at low values of q is not dominated by the plasmon, but of the dipolar contribution of the Sr $4p \rightarrow 4d$ excitation.

For LAO the corresponding spectra are presented in figure 3. The plasmon energy is 30 eV, and in this case the peak at 30 eV at lowest q indeed is dominated by the actual plasmon, even if the plasmon excitation is very broad in energy and appears thus highly damped. The notable transitions in addition to the plasmon/Compton lineshape are La $O_{1,2,3}$ transitions marked in figure 3 by vertical lines. It is notable that the La $O_{2,3}$ transitions have very similar energies to those of Sr $N_{2,3}$ in $SrTiO_3$, and the La O_1 transition very similar to that of Ti $M_{2,3}$. This renders the La lines almost invariably overlapping with different excitations in $SrTiO_3$.

The dielectric function of STO has been studied using electron energy loss and spectroscopic ellipsometry [16, 61, 62] at the low q limit. Our results provide finite q information on the excitation spectrum of LAO, STO and their multilayers at the insulating and metallic limits. The DOS, experimental $S(\vec{q}, \omega)$ and first principles response functions for STO are presented in figures 4 and 5. Before analyzing the STO spectrum, we summarise the density of states obtained from the LDA calculation. The DOS about the band gap is presented in figure 4. The energy scale was aligned so that the valence band edge is at 0 eV. The Ti 3*s* states are found at −49.4 eV, Sr 4*s* states are at −32.8 eV, and Ti 3*p* states are at −32.2 eV. There is a band from −18 eV to −16 eV with mainly O 2*s* character and small Sr 4*p* contribution. The next band ranges from −15 eV to −14 eV and is mostly comprised of Sr 4*p* states. The valence band between −5 eV and 0 eV is predominantly of O 2*p* character, with a small Ti 3*d* contribution. The first unoccupied states are at 2–10 eV and have Ti 3*d* and Sr 4*d* character. Most of the Ti 3*d* spectral weight of this band is between 2 eV and 4 eV. The Sr 4*d* states contribute predominantly in a range of 7–10 eV.

For STO, the most prominent features in the experimental loss function are at approximately 16 and 30 eV. From figure 5 we observe that Re ε has a minimum at 28 eV. Although there is no zero crossing of the real part, which would cause, by

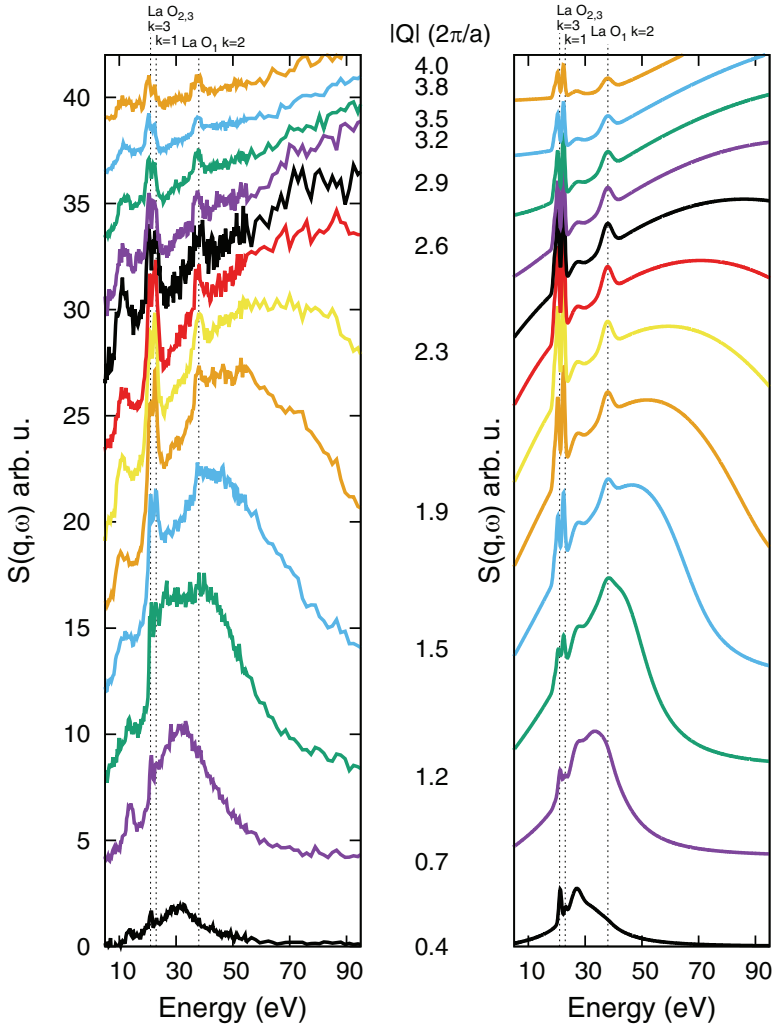

Figure 3. Similar as figure 2 but for $LaAlO_3$. (a) Experimental IXS spectra; (b) Simulated spectrum with the same offsets as in figure 2. The 21 eV peak originates from the 1*s*2*p* transition of He in the spectrometer chamber. The dashed lines mark the positions of notable semicore excitations.

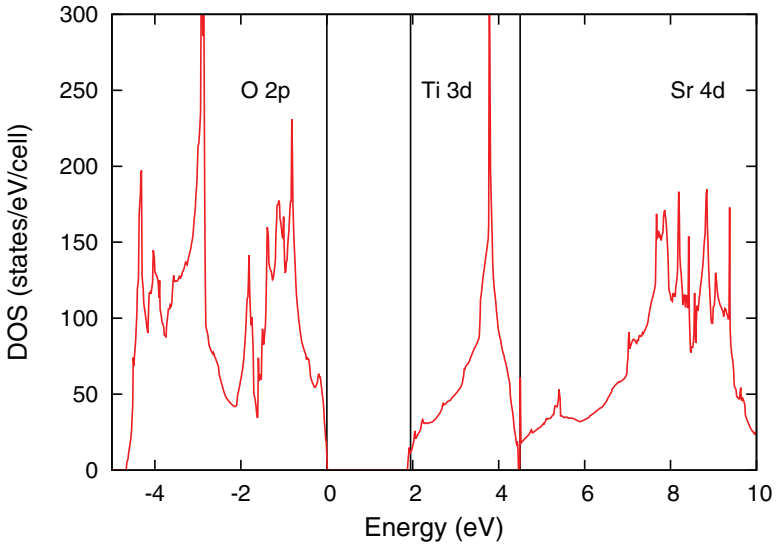

Figure 4. Valence and conduction bands for $SrTiO_3$. The vertical lines divide the energy regions according to atomic site and symmetry. The dominant component for each region is marked in the figure.

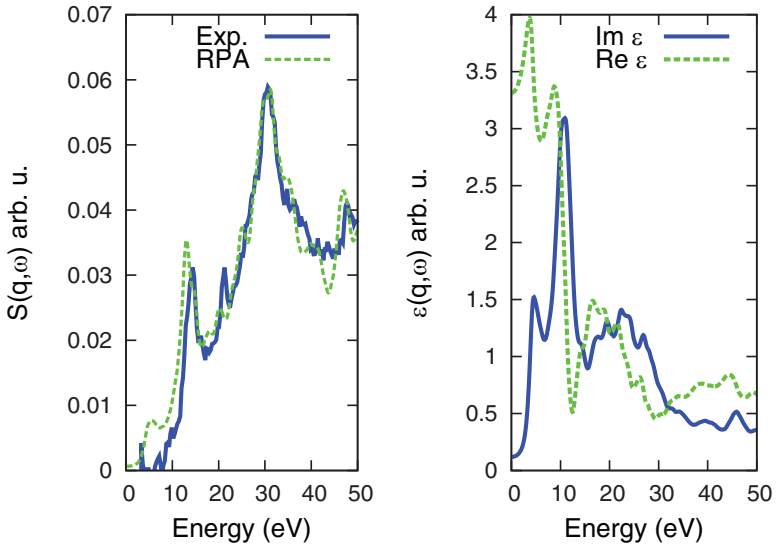

Figure 5. $SrTiO_3$ (a) Experimental IXS spectra at $\vec{q} = (0.12\vec{a}^*, 0, 0.77\vec{c}^*)$ and RPA calculation at $\vec{q} = (0.08\vec{a}^*, 0, 0.5\vec{c}^*)$; (b) Real and imaginary parts of the dielectric function.

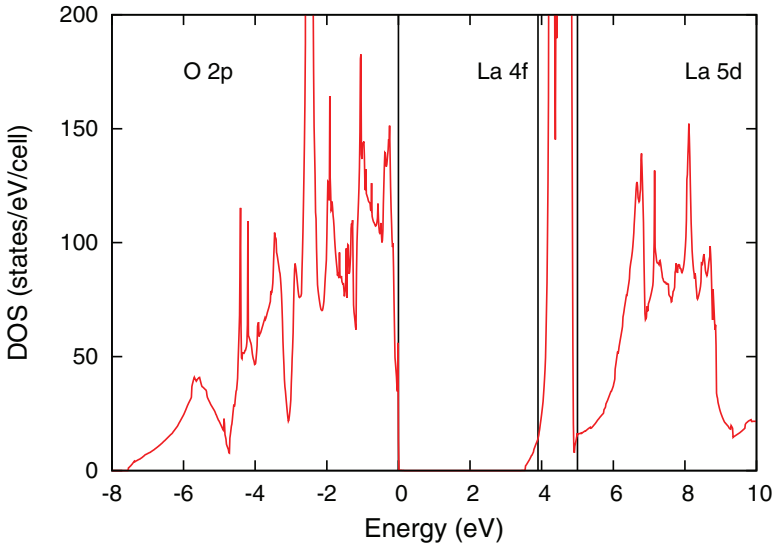

Figure 6. Valence and conduction band DOS for $LaAlO_3$. The vertical lines divide the energy regions according to atomic site and symmetry. The dominant component for each region is marked in the figure.

definition, the existence of a plasmon excitation at that point, the imaginary part is small as well, and thus the 30 eV structure is attributed to a heavily damped plasmon mixed with semicore and interband transitions. The atom centered density of states shows that the energy difference between semicore Sr 4*s* and Ti 3*p* states and the first unoccupied states also lie in this energy region, and thus provide a decay channel for the plasmon mode in addition to the more shallow valence band states. The calculated $S(\vec{q}, \omega)$ has a double peak structure at 13–15 eV. These features correspond to peaks in ε_2 and non-zero ε_1 indicating interband transitions from the Sr 4*p* valence band to unoccupied Ti 3*d* states.

The valence band density of states, experimental $S(\vec{q}, \omega)$ and response functions for LAO are presented in figures 6 and 7. The calculated DOS for LAO is summarized in the following. There is a narrow peak at −18 eV and wider flat feature between −17.2 eV and −15.4 eV. Both are dominated by O 2*s* levels with a La 5*p* contribution. A band with dominating La *p* and minor O *s*/*p* characters is at −14.5 eV to −12.7 eV. The valence bands lying between −8 eV and 0 eV are of majority O *p* character with minor contributions from La *p* and Al *s*/*p* states. The unoccupied part has a sharp La 4*f* peaks a 3.5–5 eV. The 5–10 eV states have La *d* and O *p* character. The DOS in vicinity of the band gap is presented in figure 6.

The dielectric function of LAO (figure 7) reveals again a heavily damped plasmon. Both real and imaginary parts of the dielectric function are small between 30 and 40 eV, resulting in a broad peak in $S(\vec{q}, \omega)$. The deep lying bands between −20 and −10 eV provide decay channels for the plasmon leading to strong damping. The 12 eV feature corresponds to a peak in the imaginary part, and is attributed to an interband transition from the O 2*p* derived bands to the La 5*d* band.

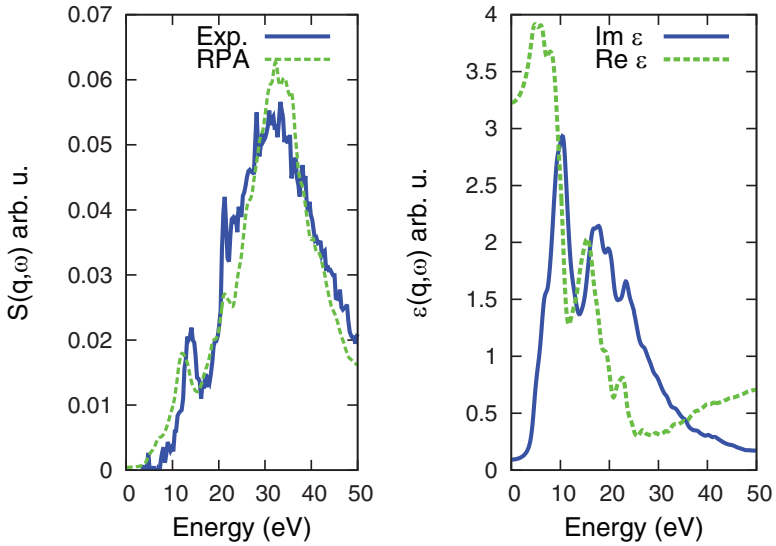

Figure 7. $LaAlO_3$ (a) Experimental IXS spectra at $\vec{q} = (0.12\vec{a}^*, 0, 0.77\vec{c}^*)$ and RPA calculation. (b) Real and imaginary parts of the dielectric function.

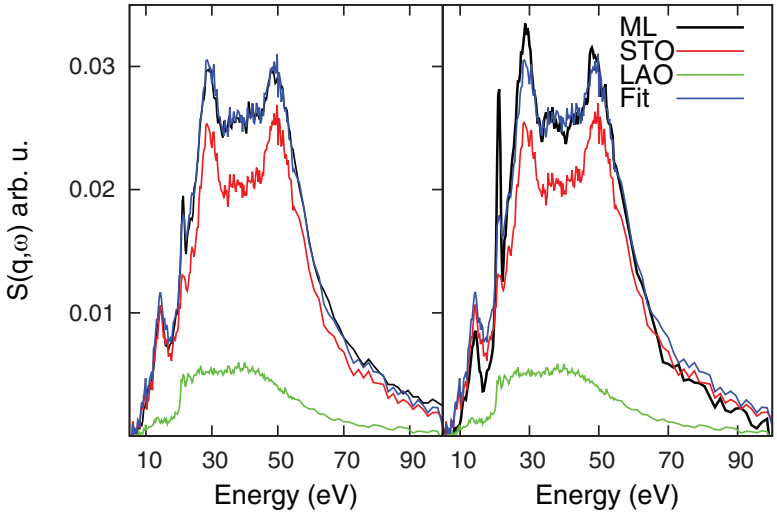

Figure 8. Left panel: Bulk spectra fitted to the ML1 sample. Right: The ML5 sample at $\vec{q} = (0.27\vec{a}^*, 0, 1.13\vec{c}^*)$.

The multilayer spectra closely resemble a superposition of the spectra of bulk STO and LAO. By fitting background-subtracted multilayer spectra from samples ML1 and ML5 with bulk spectra at the corresponding scattering angles, one obtains a STO/LAO ratio of 80:20 for the presented spectra. From this, one obtains that approximately 60% of the signal originates from the substrate and the rest from the multilayer. The fitting was performed in an energy interval of 25–70 eV to partially account for background fluctuations. Indeed it can be seen from the ML5 spectrum in figure 8 that the He 1*s* at 21 eV peak has more weight than in ML1.

It should be noted that when considering all analyzers the obtained STO fractions were found to vary between 20–80%. This is observed especially at large $\vec{q}$. The effect is readily explained by the fact that the spectra at large $\vec{q}$ is in essence the Compton continuum with partially overlapping semicore lines. This makes a least squares fit an unreliable approach at the current statistical accuracy. Thus we focus on the analysis of a more feature-rich low-q spectra, which gave consistent STO portions between samples in the fitting procedure.

As an example we present a fit to the ML1 and ML5 spectra at $\vec{q} = (0.27\vec{a}^*, 0, 1.13\vec{c}^*)$ in figure 8. The peaks remain at the same energies as in the multilayer spectra. The lineshape of the interband peak at 14–16 eV remains the same as in bulk. Similarly the main plasmon of STO and the Ti 3*s* peak at 30 and 50 eV remain bulklike. In a free electron picture one would not expect a large change in the plasmon, but the apparent similarity of the interband and semicore peaks is surprising. Valence band photoemission experiments have shown clear spectral changes for single interface samples [29]. The two sharp peaks found in the pristine STO DOS broaden and a LAO related high binding energy feature appears at −10 eV, gaining intensity as more LAO is deposited. Thus one would expect to see increased spectral weight on the high energy side of the peak. Upon closer inspection of the interband peak it is seen that the ML1 and STO peaks are identical within

statistical accuracy whereas the ML5 peak is slightly narrower. The interband peak of pristine LAO is at lower energies than in STO. It is however a very weak feature in the experimental LAO spectra at this $\vec{q}$. Recent optical conductivity experiments on thin film samples revealed a large change in the spectral region of 15–20 eV [63]. The dynamic structure factor appears not to have a similar effect, or possibly, the effects are masked by the bulk scattering contribution.

Conclusions

We have presented an experimental and computational study of the dynamical structure factor in STO, LAO and LAO/STO multilayers. The nature of the observed excitations was elucidated using a multiplet model and first principles RPA with local fields calculations. The multilayer valence spectra are well described by a superposition of bulk spectra. This implies that the changes with respect to bulk properties in both local electronic structure and long wavelength part of the Coulomb interaction (i.e. plasmons) in heterostructures are rather subtle. Whether this conclusion holds with improved experimentation or in cases where the bulk compounds have more distinct electronic structures, remains an open question. We have demonstrated that IXS is suitable for studying the neutral excitation spectra of multilayers. In comparison with resonant inelastic scattering of soft x-rays, it is possible to match the probing depth with the sample thickness via a proper choice of glancing angle and incident energy for samples thicker than the typical soft x-ray attenuation length (≈20 nm). Furthermore plasmons contribute only weakly, if at all, to the resonant IXS cross section, whereas they are a prominent feature in non resonant IXS [64]. Dipole forbidden transitions are difficult to observe in optical spectroscopies, whereas they are readily observed in IXS at large momentum transfers. We also note that x-ray standing wave effects in IXS present an interesting future direction.

A more detailed investigation of the $S(\vec{q},\omega)$ of a multilayer or thin film sample is certainly feasible. Studies of excitations below 5 eV, with $\vec{q}$ along a high symmetry lines, do not require a methodology fundamentally different from ours. Although ideal experimental conditions require the fundamentally incompatible demands of parallel beam and small footprint, modern synchrotrons and spectrometers provide enough photons on the sample and collection efficiency to allow for optimizing the beam properties for this particular application. More sophisticated calculations of $S(\vec{q},\omega)$ in heterostructures, taking lattice distortions and post-LDA exchange-correlation effects into account, could present an interesting topic for further inquiry.

Acknowledgments

We thank M Aramini and T Talka for assistance in sample characterization. Computational resources were provided by CSC—Centre for Scientific Computation Espoo, Finland. Funding was provided by the Academy of Finland (Grants 1260204, 1256211, 1127462, 1259526 and 1254065) and University of Helsinki Research Funds. T Fister was supported by the Department of Energy's Office of Science under contract award number DE-AC02-06CH11. PNC/XSD facilities at the Advanced Photon Source, and research at these facilities, are supported by the US Department of Energy—Basic Energy Sciences, the Canadian Light Source and its funding partners, the University of Washington, and the Advanced Photon Source. Use of the Advanced Photon Source, an Office of Science User Facility operated for the US Department of Energy (DOE) Office of Science by Argonne National Laboratory, was supported by the US DOE under Contract No. DE-AC02-06CH11357. MH, CB, YH and HYH acknowledge support from the Department of Energy, Office of Basic Energy Sciences, Division of Materials Sciences and Engineering, under contract DE-AC02-76SF00515. J Geck and T Ritschel gratefully acknowledge the support by the German Research Foundation through the Emmy Noether Program (Grant GE-1647/2-1) and the Research Training Group DFG-GRK 1621.

References

[1] Caliebe W A, Soininen J A, Shirley E L, Kao C C and Hämäläinen K 2000 *Phys. Rev. Lett.* **84** 3907
[2] Larson B C, Ku W, Tischler J Z, Lee C C, Restrepo O D, Eguiluz A G, Zschack P and Finkelstein K D 2007 *Phys. Rev. Lett.* **99** 026401
[3] Huotari S, Cazzaniga M, Weissker H C, Pylkkänen T, Müller H, Reining L, Onida G and Monaco G 2011 *Phys. Rev.* B **84** 075108
[4] Hiraoka N, Okamura H, Ishii H, Jarrige I, Tsuei K D and Cai Y Q 2009 *Eur. Phys. J.* B **70** 157
[5] Sternemann C, Sternemann H, Huotari S, Lehmkühler F, Tolan M and Tse J S 2008 *J. Anal. At. Spectrom.* **23** 807
[6] Caciuffo R, van der Laan G, Simonelli L, Vitova T, Mazzoli C, Denecke M A and Lander G H 2010 *Phys. Rev.* B **81** 195104
[7] Bradley J A, Gupta S S, Seidler G T, Moore K T, Haverkort M W, Sawatzky G A, Conradson S D, Clark D L, Kozimor S A and Boland K S 2010 *Phys. Rev.* B **81** 193104
[8] Gupta S S, Bradley J A, Haverkort M W, Seidler G T, Tanaka A and Sawatzky G A 2011 *Phys. Rev.* B **84** 075134
[9] Tse J S *et al* 2011 *Phys. Rev.* B **84** 184105
[10] van der Laan G 2012 *Phys. Rev. Lett.* **108** 077401
[11] van der Laan G 2012 *Phys. Rev.* B **86** 035138
[12] Gordon R A, Seidler G T, Fister T T, Haverkort M W, Sawatzky G A, Tanaka A and Sham T K 2008 *Europhys. Lett.* **81** 26004
[13] Fister T T, Fong D D, Eastman J A, Iddir H, Zapol P, Fuoss P H, Balasubramanian M, Gordon R A, Balasubramanian K R and Salvador P A 2011 *Phys. Rev. Lett.* **106** 037401
[14] Murphy B, Requardt H, Stettner J, Serrano J, Krisch M, Müller M and Press W 2005 *Phys. Rev. Lett.* **95** 256104
[15] Onida G, Reining L and Rubio A 2002 *Rev. Mod. Phys.* **74** 601
[16] van Benthem K, Elsässer C and French R H 2001 *J. Appl. Phys.* **90** 6156
[17] Cappellini G, Bouette-Russo S, Amadon B, Noguera C and Finocchi F 2000 *J. Phys. Condens. Matter* **12** 3671
[18] Sponza L, Véniard V, Sottile F, Giorgetti C and Reining L 2013 *Phys. Rev.* B **87** 235102
[19] Ohtomo A and Hwang H Y 2004 *Nature* **427** 423

[20] Thiel S, Hammerl G, Schmehl A, Schneider C W and Mannhart J 2006 *Science* **313** 1942
[21] Mannhart J and Schlom D G 2010 *Science* **327** 1607
[22] Bjaalie L, Himmetoglu B, Weston L, Janotti A and de Walle C G V 2014 *New J. Phys.* **16** 025005
[23] Li L, Richter C, Mannhart J and Ashoori R C 2011 *Nat. Phys.* **7** 762–6
[24] Bert J A, Kalisky B, Bell C, Kim M, Hikita Y, Hwang H Y and Moler K A 2011 *Nat. Phys.* **7** 767
[25] Dikin D A, Mehta M, Bark C W, Folkman C M, Eom C B and Chandrasekhar V 2011 *Phys. Rev. Lett.* **107** 056802
[26] Kalisky B, Bert J A, Klopfer B B, Bell C, Sato H K, Hosoda M, Hikita Y, Hwang H Y and Moler K A 2012 *Nat. Commun.* **3** 922
[27] Lee J-S, Xie Y W, Sato H K, Bell C, Hikita Y, Hwang H Y and Kao C-C 2013 *Nat. Mater.* **12** 703–6
[28] Willmott P R *et al* 2007 *Phys. Rev. Lett.* **99** 155502
[29] Yoshimatsu K, Yasuhara R, Kumigashira H and Oshima M 2008 *Phys. Rev. Lett.* **101** 026802
[30] Siemons W, Koster G, Yamamoto H, Harrison W A, Lucovsky G, Geballe T H, Blank D H A and Beasley M R 2007 *Phys. Rev. Lett.* **98** 196802
[31] Harrison W A, Kraut E A, Waldrop J R and Grant R W 1978 *Phys. Rev.* B **18** 4402
[32] Qiao L, Droubay T C, Varga T, Bowden M E, Shutthanandan V, Zhu Z, Kaspar T C and Chambers S A 2011 *Phys. Rev.* B **83** 085408
[33] Segal Y, Ngai J H, Reiner J W, Walker F J and Ahn C H 2009 *Phys. Rev.* B **80** 241107
[34] Müller K A and Burkard H 1979 *Phys. Rev.* B **19** 3593
[35] Koonce C S, Cohen M L, Schooley J F, Hosler W R and Pfeiffer E R 1967 *Phys. Rev.* **163** 380
[36] Schooley J F, Hosler W R and Cohen M L 1964 *Phys. Rev. Lett.* **12** 474
[37] Haeni J H *et al* 2004 *Nature* **430** 758
[38] Maurice J L *et al* 2008 *Europhys. Lett.* **82** 17003
[39] Ogawa N, Miyano K, Hosoda M, Higuchi T, Bell C, Hikita Y and Hwang H Y 2009 *Phys. Rev.* B **80** 081106
[40] Fister T T, Seidler G T, Wharton L, Battle A R, Ellis T B, Cross J O, Macrander A T, Elam W T, Tyson T A and Qian Q 2006 *Rev. Sci. Instrum.* **77** 063901
[41] Gonze Z *et al* 2009 *Comput. Phys. Commun.* **180** 2582
[42] Hartwigsen C, Goedecker S and Hutter J 1998 *Phys. Rev.* B **58** 3641
[43] Mitchell R H, Chakhmouradian A R and Woodward P M 2000 *Phys. Chem. Miner.* **27** 583
[44] Nakatsuka A, Ohtaka O, Arima H, Nakayama N and Mizota T 2005 *Acta Crystallogr.* E **61** i148
[45] Guo S-D and Liu B-G 2011 *J. Appl. Phys.* **110** 073525
[46] Peacock P W and Robertson J 2002 *J. Appl. Phys.* **92** 4712
[47] Marini A, Hogan C, Grning M and Varsano D 2009 *Comput. Phys. Commun.* **180** 1392
[48] Cowan R 1981 *The Theory of Atomic Structure and Spectra* (Berkeley, CA: University of California Press)
[49] Sternemann C, Soininen J A, Huotari S, Vankó G, Volmer M, Secco R A, Tse J S and Tolan M 2005 *Phys. Rev.* B **72** 035104
[50] Bradley J A, Moore K T, van der Laan G, Bradley J P and Gordon R A 2011 *Phys. Rev.* B **84** 205105
[51] Nyrow A *et al* 2014 *Contrib. Mineral. Petrol.* **167** 1012
[52] Nyrow A, Tse J S, Hiraoka N, Desgreniers S, Büning T, Mende K, Tolan M, Wilke M and Sternemann C 2014 *Appl. Phys. Lett.* **104** 262408
[53] Ding Y *et al* 2014 *Phys. Rev. Lett.* **112** 056401
[54] Schülke W 2001 *J. Phys. Condens. Matter* **13** 7557
[55] Schülke W 2007 *Electron Dynamics by Inelastic X-Ray Scattering* (Oxford: Oxford Science Publications)
[56] Salluzzo M *et al* 2009 *Phys. Rev. Lett.* **102** 166804
[57] Gordon R A, Haverkort M W, Gupta S S and Sawatzky G A 2009 *J. Phys.: Conf. Ser.* **190** 012047
[58] Campbell J and Papp T 2001 *At. Data Nucl. Data Tables* **77** 1
[59] Huotari S, Hämälainen K, Manninen S, Kaprzyk S, Bansil A, Caliebe W, Buslaps T, Honkimäki V and Suortti P 2000 *Phys. Rev.* B **62** 7956
[60] Huotari S, Sternemann C, Volmer M, Soininen J A, Monaco G and Schülke W 2007 *Phys. Rev.* B **76** 235106
[61] Ryen L and Olsson E 1999 *J. Appl. Phys.* **85** 2828
[62] van Benthem K, French R, Sigle W, Elssser C and Rhle M 2001 *Ultramicroscopy* **86** 303
[63] Asmara T C *et al* 2014 *Nat. Commun.* **5** 3663
[64] Ament L J P, van Veenendaal M, Devereaux T P, Hill J P and van den Brink J 2011 *Rev. Mod. Phys.* **83** 705